Journal of Molecular Structure 1201 (2020) 127208

Contents lists available at ScienceDirect

Journal of Molecular Structure

journal homepage: http://www.elsevier.com/locate/molstruc

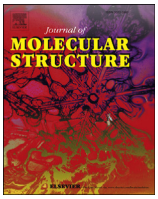

Comprehensive study on the topological properties of 5-Amino-2-Methyl Benzene Sulfonamide involving inter and intra molecular hydrogen bonds

C. Anzline [a, c], P. Sivakumar [b], S. Israel [c, *], K. Sujatha [a, d]

[a] *Research Scholar, Mother Teresa Women's University, Kodaikanal, 624 102, India*
[b] *Department of Physics, CPCL Polytechnic College, Chennai, 600 068, India*
[c] *Department of Physics, The American College, Madurai, 625 002, India*
[d] *Department of Physics, RVS School of Engineering and Technology, Dindigul, 624 005, India*

ARTICLE INFO

Article history:
Received 21 August 2019
Received in revised form
4 October 2019
Accepted 8 October 2019
Available online 11 October 2019

Keywords:
AIM analysis
Quasi rings
Intra molecular hydrogen bonds
Hirshfeld surface analysis

ABSTRACT

Density functional calculations with Becke's three parameter hybrid method using the correlation functional of Lee, Yang and Parr were carried out for the molecule 5-Amino-2-Methyl Benzene Sulfonamide with 6-311G++(d,p) basis set. Attention has been paid to explain one of the most fascinating observation of C—H···O and C—H···N intra molecular hydrogen bonds. Effect of C—H···O hydrogen bond interactions on the C—H bond length was analyzed. The network of inter and intra molecular hydrogen bonds was systematically investigated. Bader's AIM theory was used to perform the topological study of electron density. Criteria for hydrogen bonding are comprehensively reviewed for each hydrogen bond revealed, and the concept of improper blue shift hydrogen bonding is addressed.

1. Introduction

In the past few decades a real revolution took place in the field of drug engineering, where the fundamental task is to analyze the structural and electronic properties of a molecule in order to appreciate their biological role and its interactions with other molecule. One way of tackling the problem is to address it theoretically. Linus Pauling's [1] chemical bond analysis has settled the theoretical ground rules of chemical bonding and the simple notation of Lewis [2] is still applicable in all branches of chemistry. However Lewis structures depict two center two electron bonds and it is inadequate to explain much richer topologies connected with more complex bonding. Cyclic π-conjugated molecules cannot be represented by single Lewis structures and referred as delocalized. As a result resonance theory was used to describe the delocalized structures by the natural bond orbital theory [3,4].

With an endeavor of building a precise theory of chemical bonds and identifying distinct bonding patterns Bader investigated the gradient field of electron density and developed the quantum theory of atoms in a molecule (AIM) [5]. The AIM theory provides a methodology for the identification of a bond between any two atoms in a molecule in terms of bond critical points (BCP) and their properties such as electron density and it's Laplacian. Analysis according to AIM theory of theoretical and experimental electron densities for various compounds has been performed by Destro et al. (2000), Benabicha et al. (2000), Ranganathan et al. (2003), Lecomte et al. (2003), Scheins et al. (2004), Rodel et al. (2006), Kalinowski et al. (2007), Srinivasan et al. (2011) and so on [6–13].

Recently many researches are devoted to hydrogen bonds because of their essential role in bio chemical activities and biological processes [14–20]. Pauling stated that "under certain conditions an atom of hydrogen is attracted by strong forces to two atoms, instead of only one, so that it may be considered to be acting as a bond between them" [1]. Thus Hydrogen bonds come into play when a hydrogen atom is covalently bonded to a highly electronegative atom. This interaction is designated as X—H...Y, where X—H is the covalent or polar proton donation bond and H···Y is the weaker interaction. More recently, a variety of AIM based descriptors were used in the study of C—H ... X hydrogen bonding [21] and dihydrogen bonding [22]. These two publications defined a set of criteria for hydrogen bonding within AIM formalism. Moreover, the AIM formalism may be used to deal with a new concept derived

---

* Corresponding author.
E-mail address: israel.samuel@gmail.com (S. Israel).

https://doi.org/10.1016/j.molstruc.2019.127208
0022-2860/

from the closer examination of hydrogen bonds called as “improper blue shift hydrogen bonds” [23]. Those hydrogen bonds are characterized by the shortening of the C—H bond and a blue shift in C—H stretching frequency in contrast to red shifted proper hydrogen bonds [24]. This improper hydrogen bonding is intra molecular in nature. The change of X—H bond length is connected to the charge transfer from the acceptor to donor molecule which can be ascertained by means of NBO analysis [25].

The majority of X-ray structure determination still uses the spherical atom assumption. This approach is limited to the determination of atomic positions and the evaluation of distances and angles between the coordinates. On the other hand electron density distribution in a crystal is not only made up of the contributions from the spherical core but also from the aspherical distributions of the valence shell caused from chemical bonding or intra and intermolecular interactions. The widely used approach for this purpose is the Hansen-Coppens multipole formalism [26] that has gained extensive information from the diffraction experiment. It provides more exact atomic positions and detailed information about the electron density in the crystal including aspherical bonding densities [27–29].

Experimental charge densities are usually based on the multipole model. Alternatively they can be determined by the maximum entropy method (MEM) [30–33]. MEM electron densities have been used to study the disorder in crystal structures. Disorder in crystal structures can be expressed as partially occupied atomic sites. The electron density will exhibit local maxima at the partially occupied atomic site and the Anharmonic Displacement Parameters may show up as extended local maxima that trace the dynamic disorder of a particular atom. Earlier studies have stressed artifacts in MEM densities which has magnitudes equal to the deformation densities of chemical bonds and that prohibit the use of MEM in charge density studies [34,35]. But these problems have been overcome by including the pro-crystal prior density [36], use of static weights in F constraint [37], use of prior derived F constraint [38] and the definition of criterion of convergence for MEM iterations [32].

The present work deals with the investigation of the structural and electronic properties of 5-Amino-2-methylbenzene sulfonamide due to its medicinal importance. Sulfonamide compounds are largely employed in the area of pharmaceuticals and it can be used in the prevention and treatment of bacterial infections, diabetes mellitus, edema, hypertension, and gout. 5-Amino-2-methylbenzene sulfonamide is a benzoic acid derivative in which the molecules are linked into a three dimensional network through the N—H···O intermolecular interactions [39].

The properties of crystalline material strongly depend on the arrangement of the constituent components with respect to one another. Investigation of the structural stability of compounds by theoretical and experimental methods is of great interest. Density Functional Theory (DFT) has been a favorite in theoretical modeling since it has a greater accuracy in reproducing the experimental values [40,41]. It gives information regarding the structural parameters, electronic properties and orbital interaction [42,43]. The optimized molecular geometry of the chosen compound and its molecular properties such as frontier molecular orbital analysis, population analysis, molecular electrostatic potential were determined and analyzed by the Density Functional Theory employing the basis set 6311G ++(d,p). One dimensional charge density mapping was done from the experimental methods to find the spread of charge density in real space. An investigation of close intermolecular contacts between the molecules through Hirshfeld surface analysis is also presented to quantify the interactions within the crystal structure [44].

2. Computational details of DFT

The crystal structure of 5-Amino-2-methylbenzene sulfonamide has been reported earlier at room temperature [39]. The isolated molecule DFT calculations were performed using GAUSSIAN 09W. The atomic coordinates were taken from the Crystallographic Information File. The geometry of the molecules was fully optimized using the hybrid exchange correlation functional B3LYP with a double numeric plus polarization basis set. The NBO calculations were performed using NBO program as implemented in Gaussian 09W package at the DFT/B3LYP level in order to understand the intra molecular delocalization or hyper conjugation. Analysis of electron density by Bader’s theory of atoms in molecules was performed using *Multiwfn 3.3.9* (MWF) program [45].

3. Multipole refinement

The multipole model represents an extrapolation from a finite set of experimental data. An important feature of the multipole model is the possibility to adjust the radial dependence for each atom type by including the expansion/contraction controlling parameters κ in the refinement and possibly also the parameters κ' to change the radial dependence of the valence deformation density. In our study Hansen & Coppens multipole model [26] was used. Apart from structural refinement additional parameters were refined in multipole model including electron population in valence orbitals, multipoles up to hexadecapole and corresponding radial expansion parameters.

4. Maximum entropy method

Maximum Entropy Method (MEM) is one of the appropriate methods in which the concept of entropy is introduced to handle the uncertainty properly. The principle of MEM is to obtain an electron density distribution, which is consistent with the observed structure factors and to leave the uncertainities maximum. Collins [46] formulated this method for crystallographic applications where the electron density is constructed by an iterative procedure based on constrained entropy maximization.

5. Results and discussion

5.1. Structural description

The title compound belongs to an orthorhombic system (*Iba*2) with the following lattice parameters a = 10.679 Å, b = 22.431 Å, c = 7.1980 Å and $\alpha = \beta = \gamma = 90^\circ$ and a unit cell volume of 1724.2 Å^3. The optimized molecular structure together with the numbering scheme is shown in Fig. 1. In the optimized molecule the electrons are delocalized in the aromatic ring. The standard values for C—C and C—H bond in the aromatic ring are 1.39 and 1.09 Å and our theoretical calculations shows that it lies between 1.3899 and 1.3999 Å and 1.0831 to 1.0853 Å which are close to standard values [47]. In the aromatic ring the bond length between 14C—15C is 1.4054 Å which is slightly greater than the standard value of 1.39 Å. The stretch in bond length between these two atoms is due to the sulphur atom which is attached to the carbon atom 15C. The optimized bond length for 6C—14C is 1.5081 Å and it agrees well with the typical bond length of 1.53 Å. The C—H bond length in methyl group ranges from 1.0913 to 1.0934 Å and N—H bond in amide group ranges from 1.0092 to 1.0163 Å which agrees well with a standard bond length of 1.09 Å and 1.01 Å. Breakdown of the regular hexagonal symmetry of the ring is evident from the decrease in values of the bond angles 15C—14C—21C, 16C—18C—19C and the increase in the values of the bond angles 14C—15C—16C,

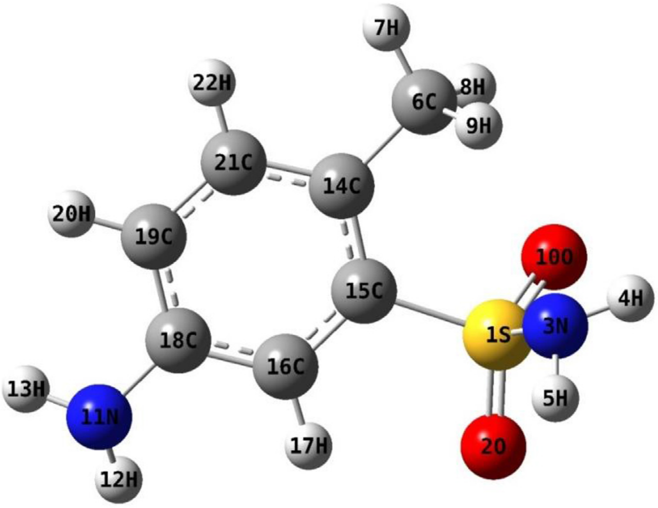

Fig. 1. Optimized molecular structure and the atom labeling scheme of 5-Amino-2-Methyl Benzene Sulfonamide.

18C—19C—21C. The breakdown of the regular hexagonal symmetry of the ring is attributed to the changes in the charge distribution on the carbon atoms. The small difference between the calculated and observed geometrical parameters can be attributed to the fact that the theoretical calculations were carried out with isolated molecules whereas the experimental values were based on the molecules in the crystalline state. The experimental and theoretical values of other important geometrical parameters can be verified from Tables 1—3.

5.2. Molecular orbital analysis

The electron cloud around the molecule is subdivided into different molecular orbitals possessed of different energy levels. The frontier molecular orbitals are very important in determining the molecular reactivity and the ability of a molecule to absorb light. The two most important frontier molecular orbitals are the highest occupied molecular orbital (HOMO) and lowest unoccupied molecular orbital (LUMO). The HOMO represents the ability to donate an electron and it has π character whereas the LUMO with π^* character has the ability to accept an electron. The HOMO-LUMO energy separation determines the kinetic stability and reactivity of the molecule. The HOMO and LUMO energies of the molecule are found to be −6.099 and −1.266 eV. The HOMO-LUMO gap of the title molecule is found to be 4.833 eV and it shows that the molecule is more polarizable and soft with high reactivity and low kinetic stability. The encapsulation of HOMO and LUMO regions in the molecule are shown in Fig. 2(a) and (b). According to Koopman's theorem [48] the HOMO and LUMO energies can be used to calculate the molecular properties. Based on the density functional theory the ionization potential, electron affinity, electronegativity, hardness, chemical potential and electrophilicity index are found to be 6.099, 1.266, 3.682, 2.416, −3.682 and 2.805 eV.

5.3. Topological analysis of theoretical charge density

AIM topological analysis was carried out using *Multiwfn 3.3.9*. Bader's AIM theory [5] affords a great tool for the qualitative analysis of the electron density $\rho(r)$ and Laplacian $\nabla^2\rho(r)$. Within the AIM theory the topology of the electron density is revealed by its gradient vector field. A series of infinitesimal gradient vectors defines a gradient path which is perpendicular to electronic iso-density surfaces and these points were converged to infinity at some points called attractors. The nucleus is called as an attractor and the paths converging to a nucleus defines a region of space called atomic basin. Some gradient paths arriving at a nucleus do not approach from infinity but from a point in between two nuclei, called a Bond Critical Point (BCP) where the gradient of $\rho(r)$ vanishes.

The critical points are characterized by two numbers, r and s, where r is the number of non zero eigen values of the Hessian matrix (rank of the critical point) and s (signature) is the algebraic sum of the signs of the eigen values. Usually for molecules the critical points are of rank 3. The four kinds of non degenerate critical points of rank 3 are maxima (3, −3), minima (3, +3) and two types of saddle points (3, +1) and (3,-1) corresponding to nuclear positions, cages, rings and bonds [49]. For a (3,-3) critical point the three eigenvalues are non zero and all negative. The position of (3, −3) local maximum is called nuclear critical point (NCP) and it is nearly identical to the nuclear positions. A critical point that is characterized by two negative curvatures and one positive curvature is labeled as (3,-1) BCP. It is maximum along the inter atomic surfaces perpendicular to the bond path (λ_1 and λ_2) and minimum along the bond path (λ_3). These BCP's link two nuclei through a unique gradient path called the bond path. In contrast, a ring critical point (RCP) has one negative curvature and two positive curvatures and it is labeled as (3, +1) which displays steric effect. The (3, +3) critical point known as the cage critical point (CCP) has the minimum of electron density and it appears in the cage system. The number and types of critical points that can exist in a system with a finite number of nuclei are governed by Poincare-Hopf relationship which is expressed as $n\,(3,-3) - n\,(3,-1) + n\,(3,+1) - n\,(3,+3) = 1$ where n represents the number of critical points of each type and

Table 1
Comparison of Theoretical and Experimental Bond lengths.

Bond	Bond Length (Å)				Bond	Bond Length (Å)			
	B3LYP/6311G ++ (d,p)	Multipole Analysis	MEM	XRD		B3LYP/6311G++ (d,p)	Multipole Analysis	MEM	XRD
1S—2O	1.4634	1.4599	1.4598	1.444	11N—13H	1.0092	0.8025	0.8025	0.861
1S—3N	1.6983	1.5942	1.5942	1.597	11N—18C	1.3952	1.3553	1.3552	1.379
1S—10O	1.4618	1.4243	1.4242	1.435	14C—15C	1.4054	1.4168	1.4168	1.416
1S—15C	1.8053	1.7912	1.7911	1.77	14C—21C	1.3989	1.4007	1.4007	1.397
3N—4H	1.0163	0.8592	0.9513	0.859	15C—16C	1.3917	1.3707	1.3707	1.386
3N—5H	1.0159	0.9017	0.9017	0.86	16C—17H	1.0831	0.9211	0.9210	0.93
6C—7H	1.0917	1.0013	1.0013	0.96	16C—18C	1.3999	1.4422	1.4421	1.405
6C—8H	0.9987	0.9956	0.9955	0.96	18C—19C	1.3998	1.4035	1.4035	1.408
6C—9H	0.9724	0.9418	0.9417	0.96	19C—20H	1.0853	1.0016	1.0015	0.931
6C—14C	1.5081	1.4748	1.4747	1.501	19C—21C	1.3899	1.3789	1.3788	1.37
11N—12H	1.0093	0.9246	0.9245	0.861	21C—22H	1.0849	1.0214	1.0214	0.93

Table 2
Comparison of theoretical and experimental bond angles.

Bond	Bond Angle (°)				Bond	Bond Angle (°)			
	B3LYP/ 6311G++ (d,p)	Multipole Analysis	MEM	XRD		B3LYP/ 6311G++ (d,p)	Multipole Analysis	MEM	XRD
2O−1S−3N	109.10	107.21	107.20	106.84	6C−14C−15C	124.45	125.61	125.60	124.78
2O−1S−10O	120.58	118.62	118.62	118.65	6C−14C−21C	120.17	120.35	120.34	119.46
2O−1S−15C	107.52	106.72	106.72	106.92	15C−14C−21C	115.37	114.01	114.00	115.71
3N−1S−10O	105.45	106.48	106.47	106.73	1S−15C−14C	121.63	119.74	119.73	121.41
3N−1S−15C	102.85	109.14	109.14	109	1S−15C−16C	115.38	115.06	115.06	116.5
10O−1S−15C	109.91	108.42	108.42	108.43	14C−15C−16C	122.94	125.13	125.13	122.06
1S−3N−4H	108.56	107.91	107.90	120.02	15C−16C−17H	119.08	121.39	121.38	119.62
1S−3N−5H	110.38	118.92	118.91	120.01	15C−16C−18C	120.29	118.67	118.67	120.69
4H−3N−5H	110.80	130.87	130.87	119.97	17H−16C−18C	120.61	119.94	119.94	119.69
7H−6C−8H	108.62	105.92	105.92	109.55	11N−18C−16C	120.69	121.34	121.33	120.92
7H−6C−9H	108.18	108.49	108.48	109.46	11N−18C−19C	121.36	121.41	121.41	121.49
7H−6C−14C	109.99	108.48	108.48	109.49	16C−18C−19C	117.87	117.24	117.24	117.58
8H−6C−9H	107.21	108.55	108.54	109.44	18C−19C−20H	119.74	119.05	119.04	119.62
8H−6C−14C	111.57	111.02	111.0178	109.44	18C−19C−21C	120.65	121.21	121.21	120.7
9H−6C−14C	111.11	114.04	114.0436	109.45	20H−19C−21C	119.59	119.62	119.62	119.67
12H−11N−13H	112.33	122.28	122.2788	119.93	14C−21C−19C	122.84	123.58	123.58	123.24
12H−11N−18C	115.84	119.19	119.1918	120.05	14C−21C−22H	118.41	114.54	114.54	118.38
13H−11N−18C	115.83	116.46	116.4627	120.01	19C−21C−22H	118.73	121.67	121.67	118.39

Table 3
Dihedral angles from DFT.

Bond	Dihedral Angle (°)	Bond	Dihedral Angle (°)	Bond	Dihedral Angle (°)
2O−1S−3N−4H	105.27	9H−6C−14C−15C	−60.1257	1S−15C−16C−18C	−178.19
2O−1S−3N−5H	−16.36	9H−6C−14C−21C	119.5556	14C−15C−16C−17H	179.83
10O−1S−3N−4H	−25.59	12H−11N−18C−16C	−23.4238	14C−15C−16C−18C	0.08
10O−1S−3N−5H	−147.23	12H−11N−18C−19C	159.4933	15C−16C−18C−11N	−177.47
15C−1S−3N−4H	−140.77	13H−11N−18C−16C	−158.1498	15C−16C−18C−19C	−0.29
15C−1S−3N−5H	97.58	13H−11N−18C−19C	24.7674	17H−16C−18C−11N	2.77
2O−1S−15C−14C	−179.68	6C−14C−15C−1S	−1.966	17H−16C−18C−19C	179.95
2O−1S−15C−16C	−1.38	6C−14C−15C−16C	179.8626	11N−18C−19C−20H	−2.44
3O−1S−15C−14C	65.21	21C−14C−15C−1S	178.339	11N−18C−19C−21C	177.41
3O−1S−15C−16C	−116.47	21C−14C−15C−16C	0.1675	16C−18C−19C−20H	−179.60
10O−1S−15C−14C	−46.70	6C−14C−21C−19C	−179.9176	16C−18C−19C−21C	0.25
10O−1S−15C−16C	131.60	6C−14C−21C−22H	0.2236	18C−19C−21C−14C	0.01
7H−6C−14C−15C	−179.89	15C−14C−21C−19C	−0.2085	18C−19C−21C−22H	179.85
7H−6C−14C−21C	−0.21	15C−14C−21C−22H	179.9327	20H−19C−21C−14C	179.86
8H−6C−14C−15C	59.47	1S−15C−16C−17H	1.5596	20H−19C−21C−22H	−0.28
8H−6C−14C−21C	−120.84				

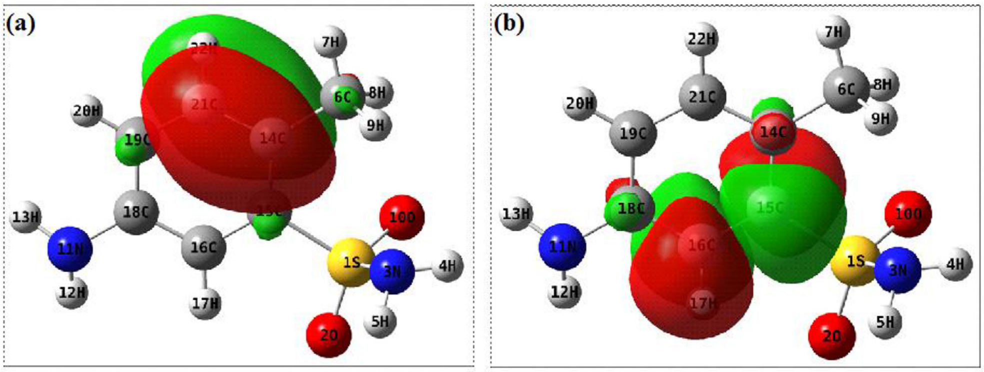

Fig. 2. Encapsulation of (a) HOMO and (b) LUMO

this equation was verified using *Multiwfn 3.3.9* (MWF) to ensure all CP's have been found. The molecular graph as revealed by AIM analysis can be visualized in Fig. 3, and it shows the bond path, bond critical point and four RCP's − one for benzene ring and the other three for the quasi rings created by intra molecular hydrogen bonds. For benzene the RCP lies in the center of the ring due to the symmetry constraints but for the other three quasi rings the RCP can be found anywhere because of the absence of symmetry. The existence of intra molecular hydrogen bonding in this molecule leads to the creation of 3 quasi rings which plays a major role in the

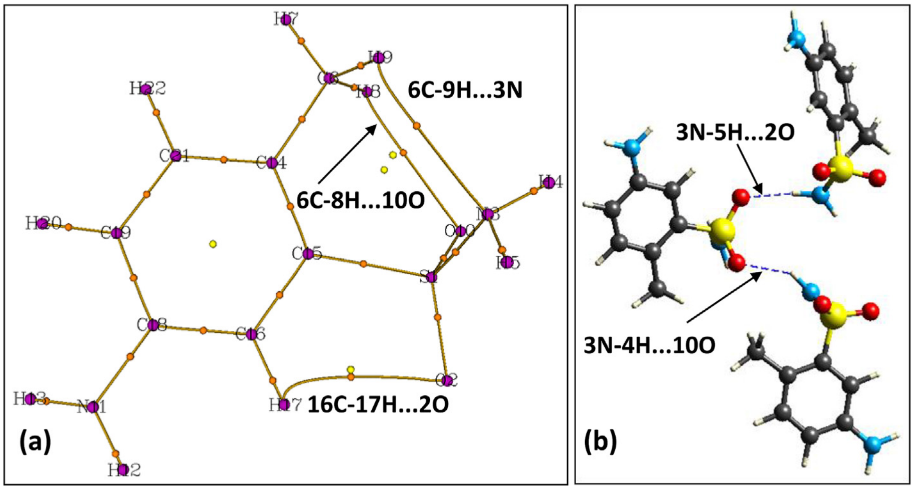

Fig. 3. (a) Molecular graph of 5-Amino-2-Methyl Benzene Sulfonamide. Large violet spheres are NCP, small orange spheres are BCP and yellow spheres in the center of the ring are RCP. Brown lines represent the bond path. The three intra molecular hydrogen bonds are highlighted. (b) Inter molecular hydrogen bonding interactions are shown by dashed lines.

bioactivity of some drugs.

The critical points are searched in the charge density distribution and are given in Table 4. The electron density $\rho_{BCP}(r)$ of the C—C bonds in the ring ranges from 0.2991 to 0.3099 e/Bohr^3. Atoms with high electronegativity have more affinity to electrons. Thus in the hetero nuclear S—O, S—N, C—S and C—N bonds, the bond critical point lies significantly closer to the S atom in S—O, S—N bond and to the C atom in C—S, C—N bonds in accordance with the greater accumulation of density concentrated in the more electronegative atom. Similar behavior is observed in hetero nuclear N—H and C—H atoms where the electronegativity for N and C atom is more compared to H atom. The difference in π character is illustrated by the change in the properties of the bond critical point for each bond type. But in the case of homo nuclear C—C bond the difference in electronegativity is zero and the bond critical point is centered between the two carbon atoms. This is evident from the d_1 and d_2 values of (3,-1) critical points and it is shown in Table 4.

One of the most attractive properties at the bond critical point is Laplacian. The Laplacian $\nabla^2\rho$ is the sum of eigenvalues of the Hessian matrix (λ_1, λ_2, λ_3) and ($\lambda_{1\text{-}3}$) are the curvatures of the electron density. The ellipticity of the bond is defined as, $\varepsilon = 1 - \ |\lambda_1/\lambda_2|$, where λ_1 and λ_2 are the principal curvatures of the electron density in the plane perpendicular to the bond ($\lambda_1 < \lambda_2 < 0$). It is a measure of departure from cylindrical symmetry at the BCP and therefore indicates the departure from pure σ bond (π character) [50].

A positive Laplacian indicates the local depletion of electron density, typical of closed shell interactions, as it occurs in ionic bonds or any other interactions like van der Waals, medium-weak hydrogen bonding etc. On the contrary the covalent bonds are typically associated with the approach of valence shell charge concentrations of the bonded charges producing a local accumulation of charge at BCP.

Table 4
Topological Analysis of (3,-1) critical point.

Bond (A1-A2)	d (Å)	d_1 (A1-CP) (Å)	d_2 (CP-A2) (Å)	ρ (e/Bohr^3)	$\nabla^2\rho$ (e/Bohr^5)	G (a.u)	V (a.u)	H (a.u)	G/ρ	V/G	ε
1S—10O	1.4617	0.5728	0.8888	0.2906	0.9016	0.5778	−0.9302	−0.3524	1.9883	1.6099	0.0196
1S—2O	1.4633	0.5732	0.8901	0.2894	0.9040	0.5758	−0.9256	−0.3498	1.9896	1.6075	0.0172
1S—3N	1.6982	0.7344	0.9641	0.2236	−0.5822	0.1089	−0.3634	−0.2545	0.4870	3.3370	0.0915
15C—1S	1.8053	0.8073	0.9980	0.1988	−0.3657	0.0462	−0.1839	−0.1377	0.2323	3.9805	0.0756
18C—11N	1.3952	0.5371	0.8584	0.2983	−0.8722	0.1603	−0.5388	−0.3784	0.5373	3.3611	0.0816
11N—12H	1.0093	0.7372	0.2721	0.3396	−1.5851	0.0571	−0.5105	−0.4533	0.1681	8.9404	0.0552
11N—13H	1.0091	0.7365	0.2726	0.3397	−1.5794	0.0575	−0.5098	−0.4523	0.1692	8.8660	0.0556
3N—4H	1.0162	0.7458	0.2704	0.3321	−1.5546	0.0555	−0.4997	−0.4442	0.1671	9.0036	0.0465
3N—5H	1.0159	0.7447	0.2712	0.3332	−1.5554	0.0554	−0.4997	−0.4443	0.1662	9.0198	0.0430
16C—18C	1.3999	0.6849	0.7150	0.3062	−0.8468	0.0981	−0.4080	−0.3098	0.3203	4.1590	0.2149
18C—19C	1.3997	0.7201	0.6797	0.3070	−0.8532	0.0983	−0.4100	−0.3116	0.3201	4.1709	0.2181
15C—16C	1.3917	0.7114	0.6802	0.3063	−0.8305	0.1046	−0.4168	−0.3122	0.3414	3.9847	0.2319
16C—17H	1.0830	0.7011	0.3819	0.2831	−0.9772	0.0372	−0.3188	−0.2816	0.1314	8.5698	0.0232
19C—21C	1.3898	0.6974	0.6923	0.3099	−0.8648	0.1018	−0.4199	−0.3180	0.3284	4.1247	0.2163
19C—20H	1.0853	0.6922	0.3931	0.2794	−0.9512	0.0398	−0.3174	−0.2776	0.1424	7.9748	0.0228
14C—15C	1.4053	0.6816	0.7240	0.2991	−0.7955	0.0991	−0.3971	−0.2980	0.3313	4.0070	0.2110
21C—14C	1.3989	0.6985	0.7003	0.3057	−0.8362	0.1001	−0.4093	−0.3091	0.3274	4.0889	0.2160
21C—22H	1.0849	0.6938	0.3910	0.2814	−0.9660	0.0386	−0.3188	−0.2801	0.1371	8.2590	0.0191
14C—6C	1.5081	0.7778	0.7302	0.2487	−0.5825	0.0596	−0.2649	−0.2052	0.2396	4.4446	0.0415
6C—7H	1.0916	0.7002	0.3914	0.2748	−0.9146	0.0432	−0.3150	−0.2718	0.1572	7.2916	0.0132
6C—8H	1.0912	0.6919	0.3994	0.2756	−0.9208	0.0409	−0.3121	−0.2711	0.1484	7.6308	0.0134
6C—9H	1.0934	0.6976	0.3957	0.2734	−0.9050	0.0422	−0.3108	−0.2685	0.1543	7.3649	0.0146
2O—17H	2.3350	1.3701	1.0193	0.0157	0.0647	0.0139	−0.0116	0.0022	0.8853	0.8345	0.1351
10O—8H	2.5362	1.4754	1.0905	0.0104	0.0351	0.0077	−0.0066	0.0010	0.7403	0.8571	0.3704
3N—9H	2.7047	1.5923	1.1223	0.0084	0.0255	0.0055	−0.0046	0.0008	0.6547	0.8363	0.3198

For the covalent X—H bonds (X = C, N) the magnitude of Laplacian increases as the X atom changes from C to N [7]. It is also noteworthy that the six C—H and the four N—H bonds have a very similar density and Laplacian at the critical point. For a typical shared shell interaction the charge density has to be large at the BCP and the Laplacian has to be negative indicating that the electronic charge is concentrated between the nuclei. Negative Laplacians observed in S—N, C—S, C—N, N—H and C—H show that the electron density is locally concentrated and it is a strong evidence of shared shell interaction but the positive Laplacian between S and O bonds predicts the depletion of electron density (See Table 4) [51,52]. High ρ(r) with positive Laplacian indicates the charge is concentrated in the inter nuclear region but spilled out of atomic basin which results in locally depleted electronic charge. This kind of interaction has been termed as intermediate between a shared and closed shell interaction, whereas the closed shell interaction exhibits a low value of ρ(r) in addition to positive Laplacian [53]. The 1S—10O and 1S—2O bond critical point has the density of 0.2906 and 0.2894 e/Bohr^3 with positive Laplacian which shows that the sulphur-oxygen bond in this compound exhibits intermediate interaction.

The spatial distribution of Laplacian along the aromatic ring, O2—S1—O10, N3—S1—O10 and H12—N11—H13 plane of the molecule is shown in Fig. 4. The local charge concentrations of all the C atoms in the ring are clearly shown as triangular in shape indicating a sp^2 —type C atom. The shared shell interaction of C—C and C—H bonds is evidently seen in Fig. 4(a). C—C and C—H bonds have high values of ρ(r) and $\nabla^2\rho(r)$ at the corresponding BCP's which can be seen from Table 4. The lone pairs around oxygen atoms can be clearly visualized from the Laplacian map of Fig. 4(b). Fig. 4(c) shows the interaction between S—O and S—N which reveals that the interaction between S—N is shared shell and S—O is intermediate. Topological analysis of (3,-1) bcp also supports this information which shows that the value for ρ and $\nabla^2\rho$ for 1S—3N bond is 0.2236 e/Bohr^3 and -0.5822 e/Bohr^5. The spatial distribution of the Laplacian in N3—S1—O10 plane shows an almost spherical distribution around oxygen atom which indicates an even distribution of electrons whereas the nitrogen atom shows more deformation in the valence region than in the core region. The local charge concentration of nitrogen atom in the amino group is triangular in shape indicating sp^2 hybridization on N atom which can be visualized from Fig. 4(d).

A local kinetic (G_{cp}) and Potential (V_{cp}) energy density functions can be defined by the first order density matrix according to Cremer and Kraka [54,55] who suggested the use of energy density at the Bond Critical Point to ascertain the nature of the chemical bond.

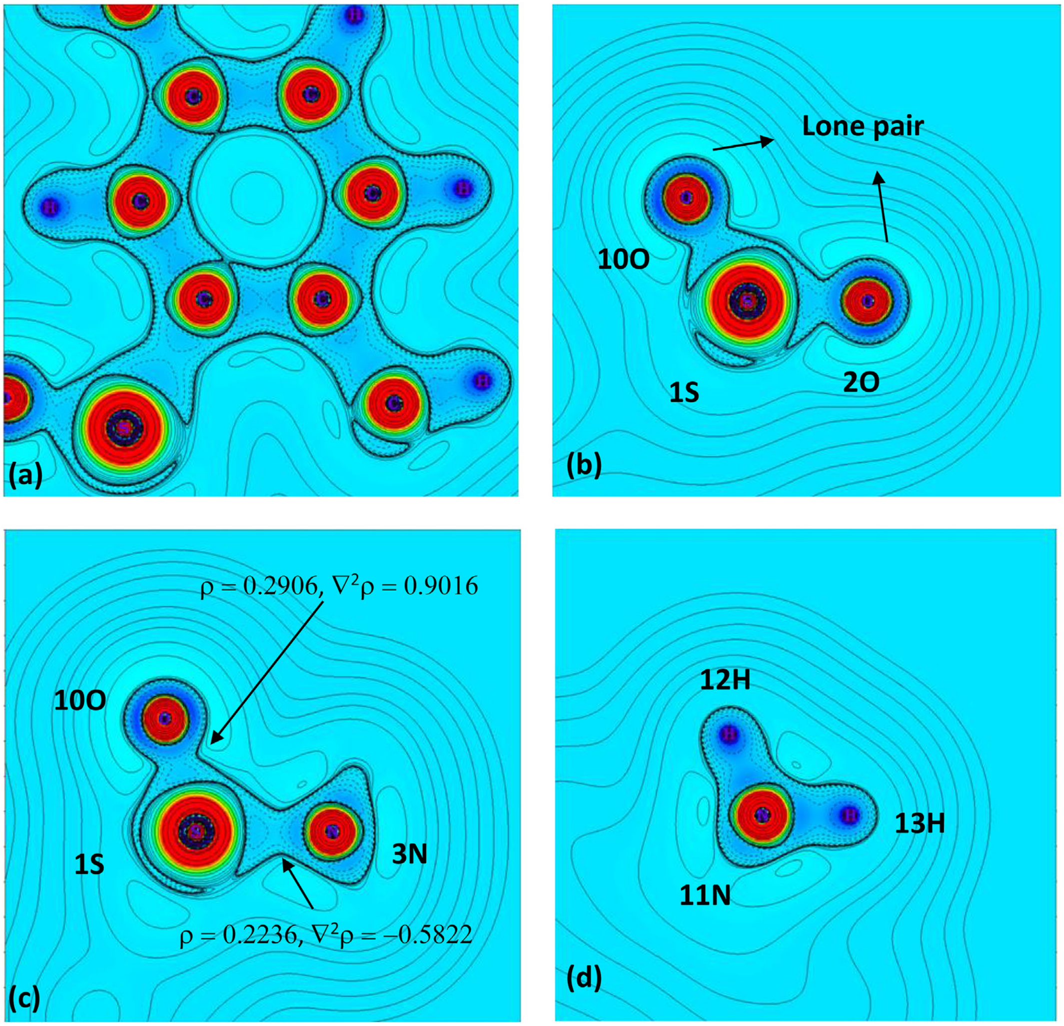

Fig. 4. The color filled map of two dimensional Laplacian along (a) Aromatic ring (b) 2O—1S—10O plane (c) 3N—1S—10O plane and (d) 12H—11N—13H plane of a molecule. Blue represents the low density region and Red represents the high density region.

The potential energy density describes the ability of the system to concentrate electrons at the BCP's while the kinetic energy density describes the tendency of the electrons to spread out in space. The total energy density H_{cp} ($=G_{cp}+V_{cp}$) reflects a dominant Covalence when $H_{cp}< 0$ (i.e. when the potential energy density is excess) whereas ionic, hydrogen bonding and van der Waals complexes have $H_{cp}\geq 0$. And the magnitude of H_{cp} reflects the degree of covalency. Furthermore the larger shared character of interaction leads to electronic stabilization of structure. It is also observed that for closed shell interaction the amount of kinetic energy per electron is large, typically $G_{cp}/\rho > 1$ a. u. The estimated G_{cp}/ρ value of S—N, C—S, C—N, N—H and C—H bonds lie between 0.1314 and 0.5373 a. u and reveals the covalent nature (shared shell interaction) of bonds. Whereas the S—O bond has a G_{cp}/ρ value of 1.98 a. u that reveals a closed shell interaction. But according to Cremer and Karka, the closed shell interaction should have a positive value for total energy density. H_{cp} values obtained from the topological analysis for the title molecule is negative and it ranges from -0.1377 to -0.4533 a. u. Thus it is impossible to predict the bonding between S and O as closed shell interaction. To understand about the interaction between S and O, the quantity (V_{cp}/G_{cp}) proposed by Espinosa et al. [56], was used to discriminate the interaction types. For closed shell or hydrogen bond interaction $V_{cp}/G_{cp} < 1$ (i.e. $H_{cp}> 0$) but for shared shell interaction the $V_{cp}/G_{cp} > 2$ (i.e. $H_{cp} < - G_{cp}$). Intermediate interaction occurs when $1 < V_{cp}/G_{cp} < 2$ ($-G_{cp} < H_{cp} < 0$). Thus the title molecule has intermediate interaction between 1S—10O and 1S—2O with a V_{cp}/G_{cp} value of 1.609 and 1.607 while all other bonds have shared shell interaction with a V_{cp}/G_{cp} value ranging from 3.337 to 9.019. The bond ellipticity ε, is known to be a good index of the π delocalization. The ε values obtained of the C—C bonds in the ring are in the range of 0.21—0.23 which is in good agreement with the calculated value in benzene 0.23 [5]. It reflects the existence of π delocalization in the benzene ring.

5.4. Inter and intra molecular hydrogen bonding from AIM theory

The existence of intermolecular hydrogen bonding is observed in the crystal between the neighboring molecules while the intra molecular hydrogen bonding occurs within two functional groups of the same molecule. Another interesting application of the topological analysis of charge density is the characterization of hydrogen bonds. Various types of hydrogen bonds like dihydrogen bonds, bifurcated hydrogen bonds, H … π interactions, and inverse hydrogen bonds were studied by Alkorta and coworkers [57—60]. In the last few decades Bader's AIM theory is often used in the analysis of hydrogen bonds and the network of hydrogen bonds present in the title molecule can be visualized from Fig. 3(a) and (b). In addition to other bonds there exists a bond path between 17H and 2O (the nearest hydrogen atom bonded to 16C), 8H and 10O (the nearest hydrogen atom bonded to 6C), 9H and 3N (the nearest hydrogen atom bonded to 6C) satisfying the density and Laplacian conditions of hydrogen bonding. The existence of the intra molecular hydrogen bond will be accepted if the H … A distance is smaller than the sum of van der Waal radii. The distance between the hydrogen and the acceptor in 16C—17H⋯2O, 6C—8H⋯10O, 6C—9H⋯3N is 2.33, 2.53, 2.70 Å which is less than the sum of van der Waal radii of H⋯O (2.72 Å) and H⋯N (2.75 Å) which confirms the existence of intra molecular hydrogen bonding. Topological analysis of hydrogen bonding is presented in Table 5. Among the five hydrogen bonds 3N—4H⋯10O and 3N—5H⋯2O has a negative Laplacian with a V_{cp}/G_{cp} value greater than two which corresponds to a shared shell or covalent interaction and they are classified as inter molecular hydrogen bonds. Whereas 16C—17H⋯2O, 6C—8H⋯10O, 6C—9H⋯3N has a positive Laplacian with a V_{cp}/G_{cp} as less than one, and a positive H value which confirms it as intra molecular hydrogen bond (See values in Table 5). Strength of the hydrogen bond depends upon the Laplacian and total energy density. If $\nabla^2\rho$ and H_{cp} are positive the bonding is weak and if it is negative the bonding is strong. Thus the strength of the intra molecular hydrogen bonding is weak compared to inter molecular hydrogen bonding which can be evident from Table 5. Three intra molecular hydrogen bonds were identified in this molecule through the AIM approach which can be viewed from the contour plot of Laplacian and it is shown in Fig. 5.

5.5. Electron localization function

The most popular alternative partition of the molecular space is provided by the topological analysis of the electron localization function (ELF), originally introduced by Becke and Edgecombe [61]. The function not only contains information on the structure of atomic shells but also clearly displays the location and size of bonding and lone electron pairs [62,63]. The ELF analysis was performed on the geometrically optimized structures using MWF. ELF depends on the excess kinetic energy D(r) caused by Pauli repulsion and the Thomas-Fermi kinetic energy density $D_0(r)$. So that ELF can be expressed as $[1+(D(r)/D_0(r))^2]^{-1}$ and its value ranges from 0 to 1. A large ELF means the electrons are greatly localized and it indicates a covalent bond, a lone pair or inner shells of an atom. Fig. 6(a) shows the ELF map of the ring where the C—C, C—N and C—S have higher values of density that show the interaction between these bonds is shared shell. Since ELF mainly depends on the kinetic energy of localized electrons it is imperative to look at the kinetic energy of the electron at BCP. The picture 6 (a) and 6 (b) and the values estimated in Table 4 depicts the interaction between S—N is shared shell and S—O is intermediate.

5.6. Population analysis

Population analysis is used to derive atomic charges and it is the simplest model to describe charge distribution. Mulliken atomic charges have an important role in the application of quantum chemical calculation to molecular systems because atomic charges affect the properties of molecular systems such as dipole moment, molecular polarizability and electronic structure. It has been used to describe the process of electronegativity equalization and charge transfer in chemical reactions. Thus the concept of atomic charges is very useful to understand the properties of molecules and it has important applications in the field of molecular modeling and drug engineering. Atomic charge analysis reveals that Mulliken scheme [64] places the negative charges among the atoms 2O, 3N, 6C, 10O, 11N, 15C, 16C, 18C and 21C while it splits the positive charges among 1S, 14C 19C and all other hydrogen atoms. Hirshfeld population [65] is the method of computing charges based on deformation density partition. It represents the charge variation in atomic space during molecule formation. These charges are too small and have poor reproducibility because the atomic dipole moments are completely neglected. In atomic dipole moment corrected Hirshfeld method (ADCH) [66], the atomic dipole moments are expanded to correct the Hirshfeld charges. In ADCH the molecular dipole moments are exactly reproduced and the atomic charges are very reasonable in chemical sense. The charges computed from Mulliken, Hirshfeld and Atomic dipole moment Hirshfeld charges are shown in Fig. 7.

5.7. Natural bond orbital analysis

Natural bond orbital analysis [67] provides an efficient method for studying intra- and inter-molecular bonding and interaction

Table 5
Topological analysis of intra and inter molecular hydrogen bonding.

D − H … A	D - H (Å)	H … A (Å)	D − A (Å)	A − H … D (°)	ρ (e/Bohr^3)	∇^2ρ (e/Bohr^5)	G (a.u)	V (a.u)	H (a.u)	V/G
3N−4H ··· 10O	1.0092	2.1583	2.9961	79.04	0.3321	−1.5546	0.0555	−0.4997	−0.4442	9.0036
3N−5H ··· 2O	1.0091	2.0221	3.0010	78.16	0.3332	−1.5554	0.0554	−0.4997	−0.4443	9.0198
16C−17H ··· 2O	1.0830	2.3350	2.8461	106.95	0.0157	0.0647	0.0139	−0.0116	0.0022	0.8345
6C−8H ··· 10O	1.0916	2.5362	3.1047	111.52	0.0104	0.0351	0.0077	−0.0066	0.0010	0.8571
6C−9H ··· 3N	1.0934	2.7047	3.3175	114.94	0.0084	0.0255	0.0055	−0.0046	0.0008	0.8363

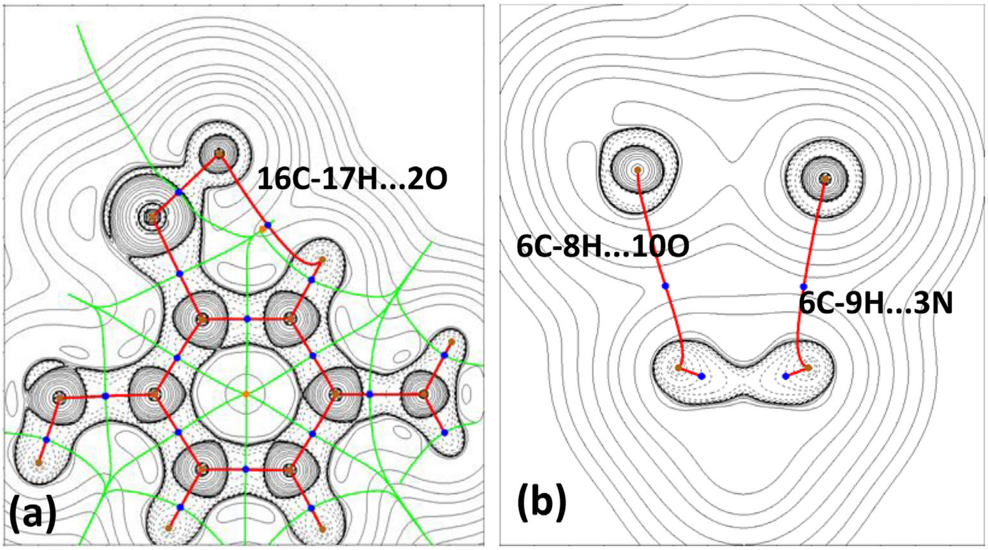

Fig. 5. Contour plot of Laplacian showing (a) 16C−17H···2O and (b) 6C−8H···10O, 6C−9H···3N intra molecular hydrogen bonds. Red lines represent the bond path and green lines inter atomic basin. Blue dots represent the BCP along the bond path.

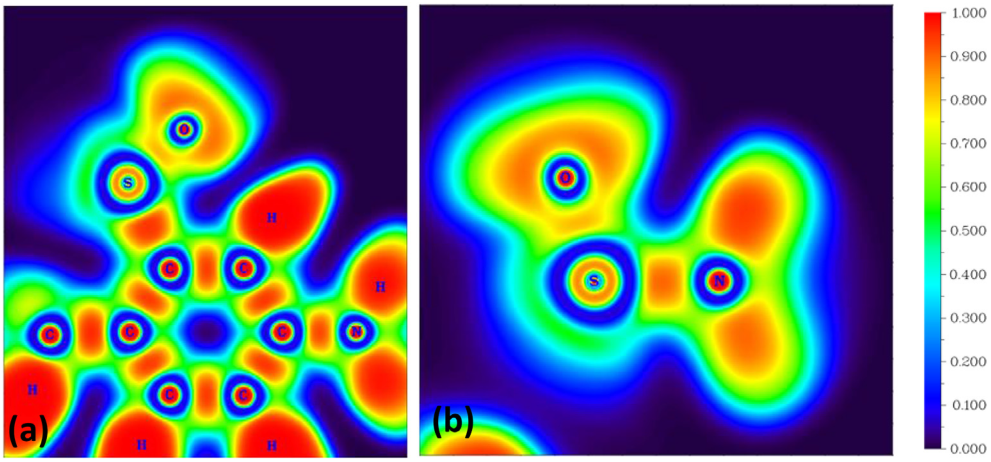

Fig. 6. ELF map of 5-Amino-2-Methyl Benzene Sulfonamide along the (a) ring and (b) 3N−1S−10O plane showing the localization and interaction in molecule.

among bonds. It partitions the electron density of a whole molecule into atomic like orbitals. The analysis is carried out by examining all possible interactions between filled Lewis type NBO's (donor) and empty non Lewis type NBO's (acceptor). Delocalization of electron density between bonding and anti bonding orbitals corresponds to a stabilizing donor-acceptor interaction and the strength of the interaction can be estimated by the second order perturbation theory. For each donor NBO (i) and acceptor NBO (j), the stabilization energy E $^{(2)}$ associated with the delocalization between donor and acceptor is estimated as $E^{(2)} = (q_i F_{i,j}^2)/(\varepsilon_j - \varepsilon_i)$, where q_i is the orbital occupancy, ε_i, ε_j are diagonal elements and $F_{i,j}$ is the off diagonal NBO Fock matrix element. The larger the E $^{(2)}$ value, the more intensive is the interaction between the electron donor and acceptor. The more the donation tendency, the greater is the extent of conjugation of the whole system. In order to elucidate the intramolecular rehybridization and delocalization of electron density NBO analysis has been performed on the title molecule at the level of B3LYP/6311G ++(d,p).

The perturbation energies of donor acceptor interactions are presented in Table 6. The intra-molecular interaction is formed by the orbital overlap between σ(1S−2O) → σ*(1S−2O), σ (1S−3N) → σ* (1S−3N), σ (1S−10O) → σ* (1S−10O) and σ (1S−15C) →σ*

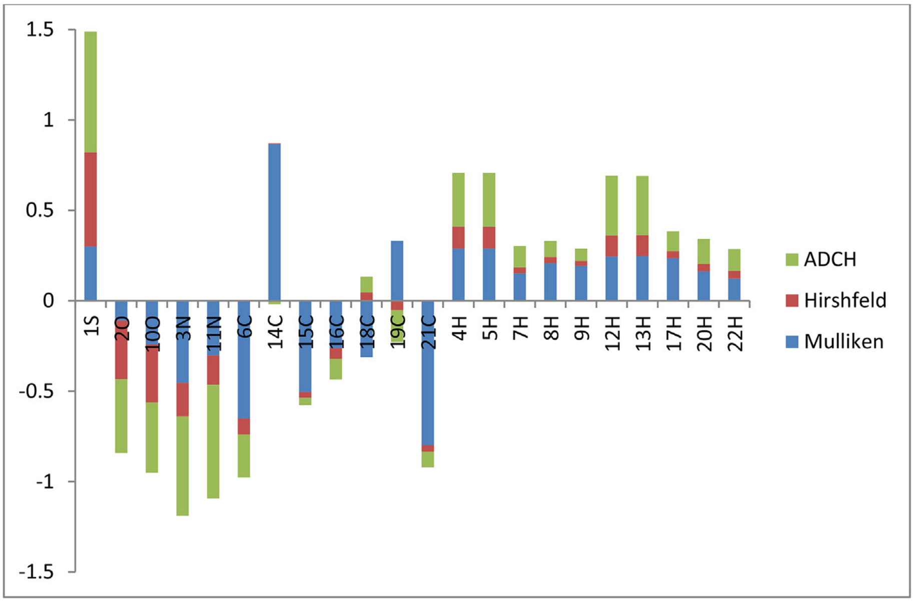

Fig. 7. Mulliken, Hirshfeld and ADCH charges calculated from 6311G++ (d,p) basis set.

Table 6
Second order interaction energy between donor and acceptor orbitals.

Donor NBO (i)	Acceptor NBO (j)	E (2) (kJmol)	E(*j*)-E(i) a.u	F (i,j) a.u	Donor NBO (i)	Acceptor NBO (j)	E (2) (kJmol)	E(*j*)-E(i) a.u	F (i,j) a.u
σ(1S–2O)	σ*(1S–2O)	3.05	1.26	0.028	π(18C–19C)	σ*(15C–16C)	87.02	0.27	0.072
σ (1S–3N)	σ* (1S–3N)	5.44	0.88	0.032	LP (1) 2O	σ* (1S–10O)	6.73	1.1	0.039
σ (1S–10O)	σ* (1S–10O)	2.67	1.27	0.026	LP (1) 2O	σ* (1S–15C)	2.93	0.97	0.024
σ (1S–15C)	σ* (1S–15C)	3.26	0.83	0.024	LP (1) 3N	σ* (1S–2O)	20.97	0.65	0.052
π (14C–21C)	π*(15C–16C)	90.37	0.26	0.068	LP (1) 3N	σ* (1S–15C)	10.59	0.52	0.033
π(14C–21C)	σ*(18C–19C)	84.01	0.27	0.067	LP (1) 3N	σ*(15C–16C)	3.01	0.39	0.016
π(15C–16C)	π*(14C–21C)	73.00	0.31	0.067	LP (1) 10O	σ* (1S–2O)	6.65	1.1	0.039
π(15C–16C)	σ*(18C–19C)	71.78	0.31	0.067	LP (1) 10O	σ* (1S–15C)	3.47	0.97	0.027
π(18C–19C)	π*(14C–21C)	90.74	0.29	0.072	LP (1) 11N	σ*(18C–19C)	110.96	0.32	0.088

(1S–15C) which results into intra-molecular charge transfer causing stabilization of the system. In the title molecule π(18C–19C) →π*(14C–21C), π (14C–21C) →π*(15C–16C), π(18C–19C) →σ*(15C–16C), π(14C–21C) →σ*(18C–19C), π(15C–16C) →π*(14C–21C), π(15C–16C) → σ*(18C–19C) has 90.74, 90.37, 87.02, 84.01, 73.00 and 71.78 kJ/mol of energy and hence they give stronger stabilization to the structure. The strong intra-molecular hyper conjugation interaction of the σ and the π electrons of the C–C to the anti C–C bond in the ring leads to the stabilization of the ring and it is evident from the data presented in Table 6. The electron donating from the lone pair 11N to anti bonding orbital σ*(18C–19C) leads to larger stabilization of 110.96 kJ/mol of energy which causes larger delocalization.

5.8. Molecular electrostatic potential

Molecular Electrostatic potential (MESP) provides more information about chemical reactivity or molecule-molecule interactions [68]. It is widely used in the study of biological recognition. Drug-receptor and enzyme-substrate interactions are two important classes of biological processes in which the initial step is recognition where the receptor recognizes the approaching molecule and promotes mutual interaction. Such recognition is believed to take place when the drug and the receptor are at a

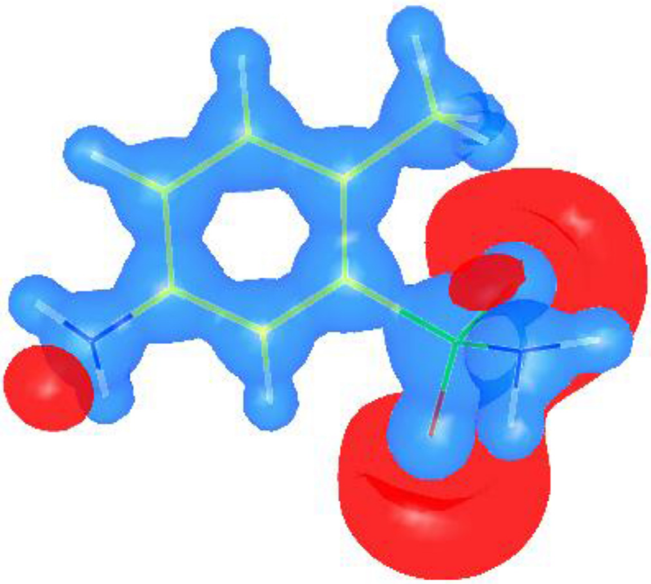

Fig. 8. Molecular electrostatic potential of 5-Amino-2-Methyl benzene sulfonamide.

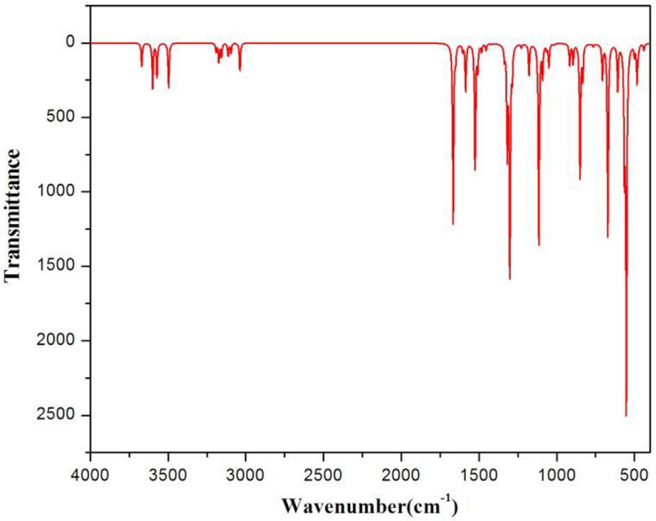

Fig. 9. Infra red Spectrum of 5-Amino-2-Methyl Benzene Sulfonamide obtained from 6311G++ (d,p) basis set.

relatively large separation and it precedes the formation of covalent bond. MESP of the title molecule is shown in Fig. 8. The red region in the lock and key model of MESP is negative and it is prone to elctrophillic attack whereas the blue region is a positive region and it is susceptible for nucleophillic attack [69]. The DFT estimations already reveal that this is a soft molecule with high reactivity and it is prone to react with other molecule that are capable of fitting themselves against electrophillic or nucleophillic region and thus qualify itself to be a good pharmaceutical compound with possible high efficacy. When this molecule docks with a bio molecule a charge transfer process can happen depending on the selective site which is either nucleophile or electrophile. The presence of intra molecular hydrogen bonding also evidences the fact that this molecule can be regarded as the candidate of bio activity. The utility of the molecule as a pharmaceutical product will be discussed elsewhere.

5.9. Hydrogen bond analysis from IR spectra

The prime tool for investigating the hydrogen bond strengthening is infrared spectral analysis. Quantum chemical calculation has been carried out for obtaining the IR vibrational spectra. The maximum number of potentially active vibrational modes of a non linear molecule which contains N atoms is (3N-6). Thus the title molecule with 22 atoms has 60 normal modes of vibration. For N atomic molecule, 2N-3 of its vibrations will be planar and the remaining N-3 will be non planar. Thus with respect to the reflections on the symmetry plane 41 of these modes will be planar (A′) and 19 will be non planar (A″). The 60 normal modes of vibrations are distributed among the symmetry species as $\Gamma_{vib} = 41A' + 19A''$ [70]. Some prominent peaks with high intensity is observed in the spectrum calculated from 6311G++ (d,p) basis set. S—N in the sulfonamide group undergoes symmetric stretching at 850.21 cm^{-1} while S=O in the same group undergoes symmetric and asymmetric stretch at 1115.21 and 1301.63 cm^{-1}. The asymmetric stretch was observed at a higher wave number than the symmetric stretch. The N—H in the amino group gives rise to two wagging and one asymmetric vibration at 552.02, 1666.17 and 3669.22 cm^{-1}. The bands observed at 671.30, 1585.86, 1090.68, 3496.40 and 3599.39 cm^{-1} have been assigned to two vibrations for N—H wagging and one vibration for N—H twisting, symmetric and asymmetric stretching in the sulfonamide group. The strong peak at 552.02 and 671.30 cm^{-1} is assigned to wagging of N—H vibrations. For the methyl group the symmetric and asymmetric stretch in C—H vibrations occurs at 3037.96 and 3095.29 cm^{-1}. The C—H stretch was found to be blue shifted by 157.96 and 125.29 cm^{-1}. This can be visualized from Fig. 9. The blue shift or hypsochromic shift is due to the rehybridization in C—H bond. Rehybidization occurs due to the polarization of C—H bond upon interaction, which increases the positive charge on the H and the negative charge on the C. In the methyl group 8H and 9H were involved in hydrogen bonding and the bond length for 6C—8H and 6C—9H was found to be 0.9956 and 0.9418 Å which is little less compared with the standard bond length of 1.09 Å. The contraction in bond length

Table 7
Isotropic displacement thermal parameters and population parameters.

Atom	Uiso (Å^2)	P10	P20	P22+	P30	P32+	P40	P42+	P44+
1S	0.0336	0.2795	−0.0277	−0.0183	0.4914	−0.3791	−0.3622	−0.0734	−0.1039
2O	0.0475	0.1145	−0.0584	−0.1014	−0.0779	−0.0784	−0.2267	0.0919	−0.0058
10O	0.0477	−0.0611	0.1885	0.0216	0.0276	0.0416	−0.1881	0.0175	−0.1097
3N	0.0460	−0.0221	−0.1025	0.0561	0.1886	−0.0090	−0.0417	−0.0123	0.0200
11N	0.0471	−0.0672	0.1789	0.2092	0.1071	−0.1212	0.2146	−0.1364	−0.0725
6C	0.0481	−0.2233	0.2230	0.0319	0.2662	−0.0357	−0.1438	0.0690	−0.1630
14C	0.0330	0.0286	0.0752	0.1017	−0.1905	−0.0528	−0.0195	−0.1444	0.0125
15C	0.0291	0.0208	−0.0917	0.0408	0.0650	0.0040	0.1561	0.0195	−0.1855
16C	0.0327	0.1954	−0.1307	0.0864	−0.0613	0.0499	0.1275	−0.2201	−0.0564
18C	0.0325	0.0330	−0.0192	0.0325	0.1169	−0.0985	−0.0820	0.0067	−0.0883
19C	0.0359	−0.0925	0.0300	0.0081	0.0662	−0.0692	0.0253	−0.0176	0.0589
21C	0.0389	−0.0412	0.0370	−0.0306	0.1567	0.0837	−0.0498	0.0632	−0.1914
4H	0.0662	0.1814	0.0076	−0.0538	−0.3628	−0.1929	−0.2598	0.1999	−0.0680
5H	0.1071	−0.2081	0.1465	−0.2397	−0.3687	0.4180	0.2493	−0.1265	−0.0599
7H	0.0548	−0.1051	−0.0185	0.1528	0.0998	0.0418	−0.2107	0.0732	−0.1713
8H	0.0855	−0.1255	0.1473	−0.0298	−0.103	0.4699	−0.1844	0.5457	−0.2364
9H	0.0245	−0.1675	−0.0315	−0.0908	0.1841	0.0953	−0.1892	0.3334	0.1776
12H	0.0375	−0.0695	0.0058	0.1732	−0.2070	−0.0138	0.2033	−0.6964	0.1464
13H	0.1597	−0.1971	−0.0571	0.2171	−0.2500	−0.6060	0.2887	−0.2065	0.1545
17H	0.0636	−0.0346	−0.0136	0.0298	−0.0052	−0.2877	−0.3317	−0.1767	0.2110
20H	0.0798	−0.0736	−0.2211	0.0678	−0.2169	−0.2282	0.2022	−0.0865	0.0057
22H	0.0580	0.0312	0.1794	−0.0263	0.1359	−0.0426	−0.0490	0.2578	−0.3676

Table 8
Experimental and theoretical core and valence charges.

Atom	P_c		P_v		κ	N_{val} -P_v	
	B3LYP/6311G++ (d,p)	Multipole Analysis	B3LYP/6311G++ (d,p)	Multipole Analysis	Multipole Analysis	B3LYP/6311G++ (d,p)	Multipole Analysis
1S	9.9985	9.9304	5.6134	6.1978	0.9305	0.3866	−0.1978
2O	1.9998	2.0244	6.9099	6.1046	0.9856	−0.9099	−0.1046
10O	1.9998	1.9927	6.9034	6.1008	0.9901	−0.9034	−0.1008
3N	1.9995	1.9841	6.0163	5.6669	0.9988	−1.0163	−0.6669
11N	1.9994	1.9959	5.7713	5.1708	0.9576	−0.7713	−0.1708
6C	1.9992	1.9619	4.5911	4.5298	0.9239	−0.5911	−0.5298
14C	1.9989	2.0405	4.0290	3.9154	1.0010	−0.0290	0.0846
15C	1.9986	1.9529	4.2167	4.3308	0.9710	−0.2167	−0.3308
16C	1.9989	1.9999	4.2165	4.0361	0.9968	−0.2165	−0.0361
18C	1.9989	1.9658	3.8171	3.9996	1.0106	0.1829	0.0004
19C	1.9990	1.9776	4.2081	4.4365	0.9468	−0.2081	−0.4365
21C	1.9990	2.0124	4.1576	3.9606	1.0158	−0.1576	0.0394
4H	0	0	0.6019	0.9198	1.1788	0.3981	0.0802
5H	0	0	0.6062	0.7906	1.1554	0.3938	0.2094
7H	0	0	0.7955	0.9494	1.1707	0.2045	0.0506
8H	0	0	0.7640	0.8559	1.1324	0.2360	0.1441
9H	0	0	0.7766	0.7359	1.1503	0.2234	0.2641
12H	0	0	0.6213	0.7389	1.1618	0.3787	0.2611
13H	0	0	0.6237	0.9130	1.1823	0.3763	0.0870
17H	0	0	0.7602	0.8072	1.1364	0.2398	0.1928
20H	0	0	0.7945	0.9316	1.1679	0.2055	0.0684
22H	0	0	0.7930	0.9504	1.1748	0.2070	0.0496

makes the charge of 6C atom to be more negative compared to all other carbon atoms and also the strength of the bond increases. The contraction in bond length increases the strength of the bond and the peak wave number is shifted to higher value which is an evidence for hydrogen bonding due to rehybridization and it exhibits improper hydrogen bond called as intra molecular hydrogen bonding. This can also be evident from Table 5.

5.10. Population parameters and atomic charges from multipole model

Experimental charge densities can be used to analyze a range of problems in chemical interest since it is a physically observable quantity. The data was collected at Enraf-Nonius CAD-4 diffractometer with an X-ray wavelength of 0.71073 Å. The multipole refinement was carried out within the Hansen-Coppens formalism using the package JANA 2006 after the successful refinement of the structural parameters [71].

The multipole deformation functions allowed for the orthorhombic site symmetry are P10, P20, P22+, P30, P32+, P40, P42 + and P44+, while the other terms vanish due to the site symmetry. The κ for 14C, 18C, 21C and all hydrogen atoms is greater than one which reveals that all these atoms undergo contraction while bonding and the valence charges decreases. Whereas the atoms like 1S, 2O, 10O, 3N, 11N, 6C, 15C, 16C and 19C undergo expansion during the bond formation and the valence charges increases. The concept of atomic charges gives powerful insights towards the understanding of physical properties and chemical reactivity. There is no clear definition of the true atomic charge however the N_{val}-P_{val} values can be considered as atomic charges obtained by crystallographic fitting in the reciprocal lattice space. The valence populations transferred from the database and after refinement with MOLLY are presented in Table 7. The N_{val}-P_{val} values cannot be considered as the total atomic charges as the multipoles also contribute to the electron transfer from one atom to other. The O and N atoms have negative N_{val}-P_{val} charges as expected and hydrogen atoms have positive charges. But in the case of carbon atoms the values of N_{val}-P_{val} are not in good agreement as they are sometimes have opposite signs. As there are four electrons involved in the covalent bonding of C atoms, the impact of the

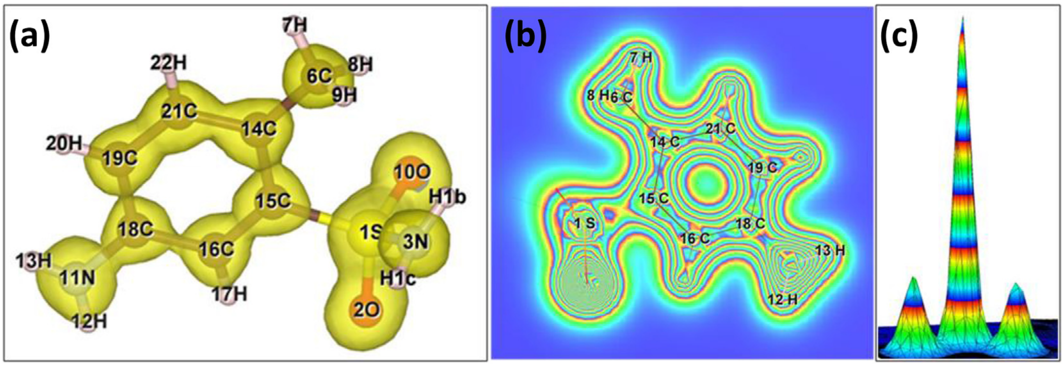

Fig. 10. (a) Three dimensional charge density distribution of the molecule at an isosurface level of 1.25 obtained from MEM (b) 2D map of aromatic ring with a contour interval of 0.5 eÅ^{-3}, (c) Relief map of 2O—1S—10O plane of the molecule.

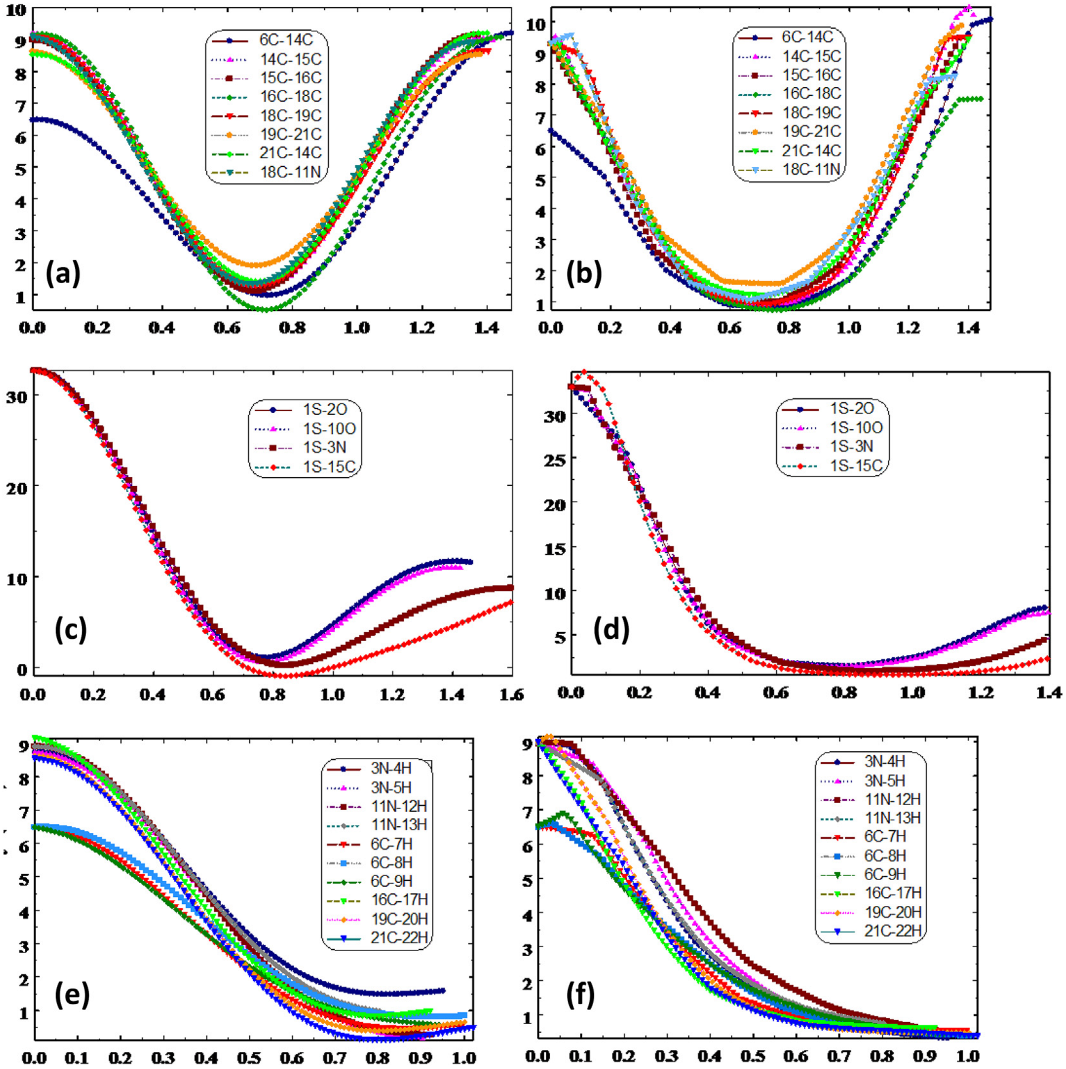

Fig. 11. One dimensional charge density profile from Multipole and MEM. Abscissa denotes the Distance (Å) and ordinate denotes the electron density (e/Å^3).

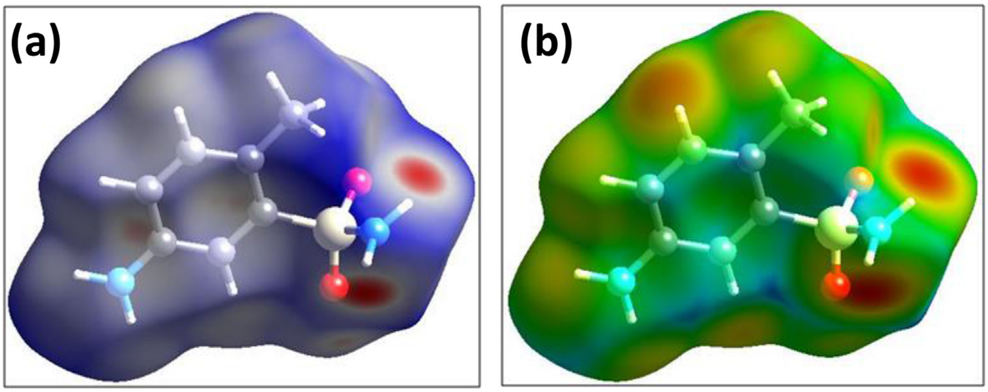

Fig. 12. Hirshfeld surface mapped with (a) d_{norm} and (b) d_i.

multipoles on the total charge is high. The N_{val}-P_{val} charges obtained from the multipole model and the theoretical model is shown in Table 8.

5.11. Charge density along the bond path

The structure factors obtained from multipole model were further utilized for MEM charge density. The three dimensional charge density of the molecule and the two dimensional charge density of the ring obtained from MEM are presented in Fig. 10 (a) and (b). The resultant charge density distribution can give accurate information about the bonding especially in the valence region. The figure plotted at the isosurface level of 1.25 shows the unique charge density of the valence region arranged in the direction perpendicular to the bond path. A clear visualization of this valence charge for the plane 2O—1S—10O is made possible in the relief map shown in Fig. 10(c) which is plotted in the range of 0.2—1.3e/Å^3. These figures clearly indicate that the bonding charges actually exists perpendicular to the bonding direction.

One dimensional charge density profile obtained from Multipole and MEM model for C—C, C—N, S—O, S—N, S—C, N—H and C—H bonds were shown in Fig. 11. These are plotted to find the size of the bonding charge and their spread in space. The presence of a local maxima or (3,-3) critical point at the position of the nucleus is a dominant topological feature of the charge density distribution. The (3,-1) critical point is found between every pair of nuclei and those two pairs are considered to be bonded to one another and the charges are accumulated all along the line linking the nuclei. The maximum electron density for the atoms 6C, 14C, 15C, 16C, 18C, 19C, 21C, 3N and 11N at the position of the nuclei are found to be 6.48,

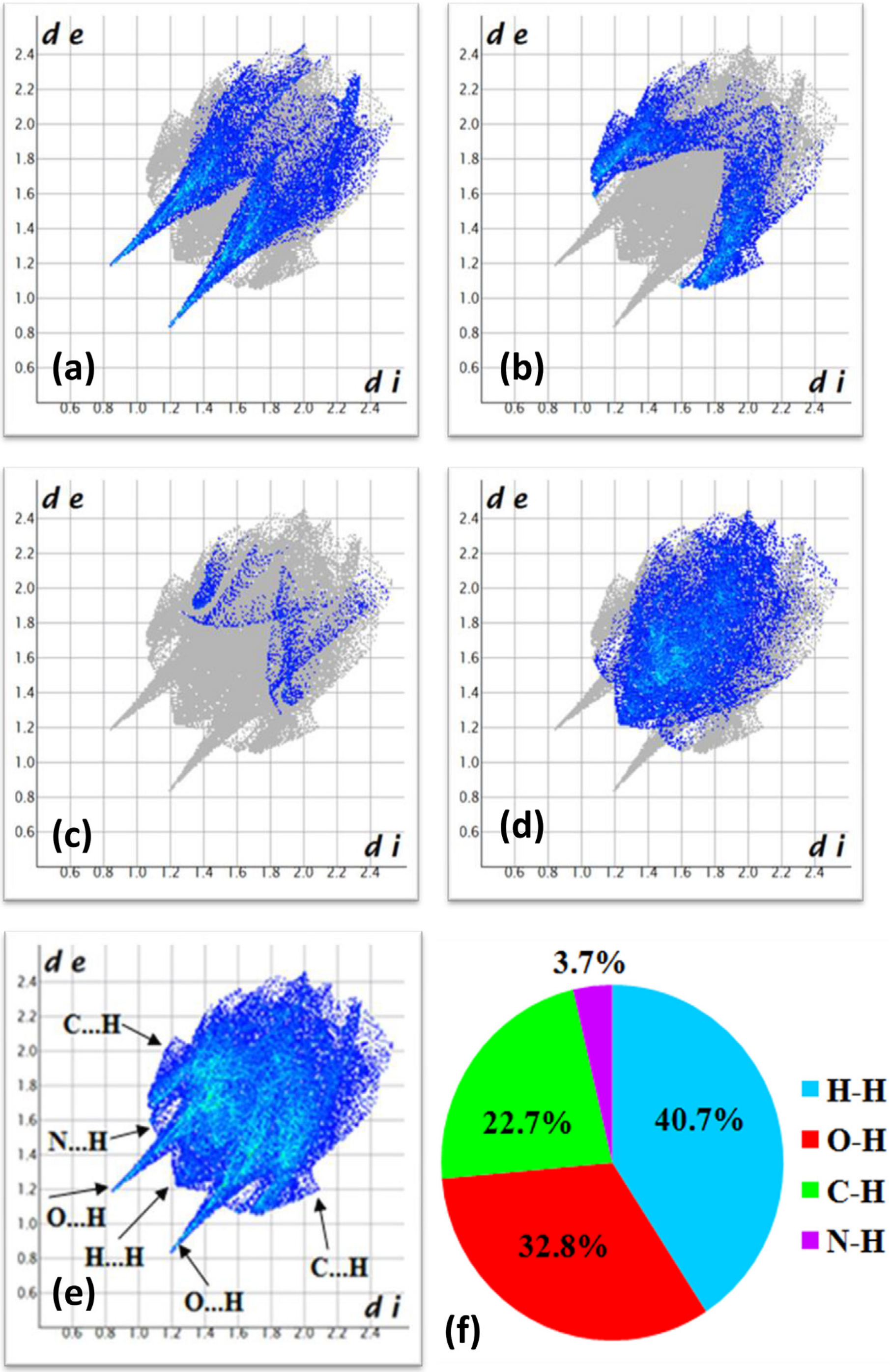

Fig. 13. 2D fingerprint plots resolved into (a) O⋯H/H⋯O, (b) C⋯H/H⋯C (c) N⋯H/H⋯N (d) H⋯H (e) full (f) percentage contribution of various intermolecular contacts.

9.20, 8.99, 9.15, 9.07, 8.62, 8.53, 8.72 and 8.90 e/Å^3. And the region of bonding charges for 6C—14C, 14C—15C, 15C—16C, 16C—18C, 18C—19C, 19C—21C, 21C—14C and 18C—11N extends up to 1.47, 1.41, 1.37, 1.44, 1.40, 1.37, 1.40, and 1.35 Å. In the homo nuclear C—C bond the BCP is centered between the two carbon atoms as there is no difference in electronegativity. The size of the carbon atom can very well be understood from the spread of the charge density along the bond path which varies between 0.707 and 0.757 Å which is comparable to the covalent radius of carbon atom (0.77 Å). In the hetero nuclear S—O, S—N, C—S, C—N, N—H and C—H bonds the strength of interaction is different and the BCP is shifted in accordance with a greater accumulation of density in the more electronegative atom.

5.12. Hirshfeld surface analysis

Each molecule in the asymmetric unit of a given crystal structure will have a unique Hirshfeld surface [72]. Hirshfeld surface is calculated using crystal explorer [73] which accepts the structure input file in CIF format. It provides a three dimensional picture of close contacts in a crystal and these contacts can be summarized in a fingerprint plot. The distance from the Hirshfeld surface to the nearest atoms outside and inside the surface are characterized by the quantities d_e and d_i and the normalized contact distance d_{norm}. The mapping of d_{norm} on the Hirshfeld surface highlights the donor and acceptor equally and it is a powerful tool for analyzing intermolecular interactions such as hydrogen bonds and C—H … π weaker contacts.

Hirshfeld surface of the title molecule was analyzed to clarify the nature and strength of inter molecular interactions. The surfaces are shown as transparent to allow visualization of molecular moiety. Hirshfeld surface mapped with d_{norm} and d_i were shown in Fig. 12. The large and deep red spots on the 3D Hirshfeld surface indicate the close contact interactions responsible for hydrogen bond contacts and the light red spots on the surfaces represent C—H … π contacts. The 2D fingerprint plots that decomposed to highlight particular atoms close pair contact is shown in Fig. 13. The O···H/H···O inter molecular interactions appears as distinct spikes in the fingerprint plot. Sets of diffuse points between the spikes are from H···H contacts. The upper wing shaped features can be recognized for C—H … π interactions and the inner wing shaped structure for N···H/H···N interactions. The contribution of intercontacts to the Hirshfeld surface for H···H, O···H/H···O, C···H/H···C, N···H/H···N was found to be 40.7%, 32.8%, 22.7% and 3.7% which revealed that the main inter molecular interaction is H···H interactions and it is shown in Fig. 13(f).

6. Conclusion

To gain better understanding on the peculiar behavior of the molecule and to interpret the interactions in the molecule AIM topological analysis was carried out. This crystallographic exploration has provided exhaustive information about the electron density distribution in the molecule. A quantitative analysis of the shared shell interaction and hydrogen bonds has been obtained through the topological analysis of total electron density. All topological and energetic properties calculated in this work are equivalent to those found in a previous study concerning X—H…O (X = C, N, O) hydrogen bonded systems. The blue shifts in the C—H stretching vibrations are due to the formation of improper intra molecular hydrogen bonding and the presence of intra molecular hydrogen bonding plays a major role in the bioactivity of drugs. These ideas definitely need further exploration and the present study is the milestone in the quest.

Declaration of competing interest

We do not have conflict of interest with any party.

References

[1] L. Pauling, The Nature of the Chemical Bond, Cornell Univ. Press, 1960.
[2] G.N. Lewis, Valence and the Structure of Atoms and Molecules, Dover, New York, 1966.
[3] J.P. Foster, F. Weinhold, J. Am. Chem. Soc. 102 (1980) 7211—7218.
[4] J.T. Nelson, W.J. Pietro, Inorg. Chem. 28 (1989) 544—548.
[5] R.F.W. Bader, Atoms in Molecules: A Quantum Theory, Oxford Univ. Press, 1990.
[6] R. Destro, P. Roversi, M. Barzaghi, R.E. Marsh, J. Phys. Chem. A 104 (2000) 1047—1054.
[7] F. Benabicha, C. Pichon-Pesme, C. Jelsch, C. Lecomte, A. Khmou, Acta Crystallogr. B56 (2000) 155—165.
[8] Anupama Ranganathan, G.U. Kulkarni, C.N.R. Rao, Probing the hydrogen bond through experimental charge densities, J. Mol. Struct. 656 (2003) 249—263.
[9] Lecomte Claude, Souhassou Mohammed, Pillet Sebastien, Topology of experimental charge density: a tool for understanding atomic interactions, J. Mol. Struct. 647 (2003) 53—64.
[10] S. Scheins, B. Dittrich, M. Messerschmidt, C. Paulmann, P. Luger, Acta Crystallogr. B60 (2004) 184—190.
[11] E. Rodel, M. Messerschmidt, B. Dittrich, P. Luger, Org. Biomol. Chem. 4 (2006) 475—481.
[12] R. Kalinowski, B. Dittrich, C.B. Hubschle, C. Paulmann, P. Luger, Acta Crystallogr. B63 (2007) 753—767.
[13] P. Srinivasan, S.N. Asthana, R.B. Pawar, P. Kumaradhas, Struct. Chem. 22 (2011) 1213—1220.
[14] G. Gilli, P. Gilli, J. Mol. Struct. 552 (2000) 1.
[15] P. Gilli, V. Bertolasi, V. Ferretti, G. Gilli, J. Am. Chem. Soc. 122 (2000) 10405.
[16] P. Gilli, V. Bertolasi, L. Pretto, V. Ferretti, G. Gilli, J. Am. Chem. Soc. 126 (2004) 3845.
[17] P. Gilli, V. Bertolasi, L. Ferretti, L. Antonov, G. Gilli, J. Am. Chem. Soc. 127 (2005) 4943.
[18] M.G. Viloca, A.G. Lafont, J.M. Lluch, J. Am. Chem. Soc. 119 (1997) 1081.
[19] S. Wojtulewski, S.J. Grabowski, J. Mol. Struct. 621 (2003) 285.
[20] A. Mohajeri, J. Mol. Struct. 678 (2004) 201.
[21] U. Koch, P.L.A. Popelier, J. Phys. Chem. 99 (1995) 9747.
[22] P.L.A. Popelier, J. Phys. Chem. A 102 (1998) 1873.
[23] E. Cubero, M. Orozco, P. Hobza, F. Luque, J. Phys. Chem. A 103 (1999), 6394, 6286.
[24] P. Hobza, Z. Havlas, Chem. Rev. 100 (2000) 4253.
[25] A.E. Reed, L.A. Curtiss, F. Weinhold, Chem. Rev. 88 (1988) 899—926.
[26] N.K. Hansen, P. Coppens, Acta Crystallogr. A34 (1978) 909—921.
[27] T.S. Koritsanszky, P. Coppens, Chem. Rev. 101 (2001) 1583—1628.
[28] Regis Guillot, Nicolas Muzet, Slimane Dahaoui, Claude Lecomte, Christian JelschActa Cryst B57 (2001) 567—578.
[29] P. Coppens, Phys. Rev. Lett. 35 (1995) 98.
[30] M. Sakato, M. Sato, Acta Crystallogr. A46 (1990) 263—270.
[31] A. Hofmann, R. Kalinowski, P. Luger, S. Van Smaalen, Acta Crystallogr. B63 (2007) 633—643.
[32] A. Hofmann, J. Netzel, S. Van Smaalen, Acta Crystallogr. B63 (2007) 285—295.
[33] J. Netzel, A. Hofmann, S. Van Smaalen, CrystEngComm 10 (2008) 335—343.
[34] W. Jauch, A. Palmer, Acta Crystallogr. A49 (1993) 590—591.
[35] W. Jauch, Acta Cryst. A50 (1994) 650—652.
[36] R. Y. de Vries, W. Briels, D. Feil, Phys. Rev. Lett. 77 (1996) 1719—1722.
[37] R. Y. de Vries, W. Briels, D. Feil, Acta Cryst. A50 (1994) 383—391.
[38] L. Palatinus, S. Van Smaalen, Acta Crystallogr. A61 (2005) 363—372.
[39] Xiang-Jun Ma, Fang Zheng, Li-Li Ren, Ping Wei, Acta Crystallogr. E65 (2009) o1815.
[40] G. Fitzgerald, J. Andzelm, Phys. Chem. 95 (1991) 10531.
[41] T. Ziegler, Pure Appl. Chem. 63 (1991) 873.
[42] J. Andzelm, E. Wimmer, J. Chem. Phys. 96 (1992) 1280.
[43] R.M. Dickson, A.D. Becke, J. Chem. Phys. 99 (1993) 3898.
[44] Saikat Kumar Seth, Gopal Chandra Maity, Tanusree Kar, J. Mol. Struct. 1021 (2012) 89—94.
[45] T. Lu, F. Chen, J. Comput. Chem. 33 (5) (2012) 580—592.
[46] D.M. Collins, Nature 298 (1982) 49.
[47] P. Sykes, A Guidebook to Mechanism in Organic Chemistry, " sixth ed., 1986.
[48] T.A. Koopmans, Physica 1 (1933) 104.
[49] R.F.W. Bader, H. Essen, J. Chem. Phys. 80 (1984) 1943.
[50] Senastin Pillet, Souhassou Mohamed, Claude Lecomte, Acta Crystallogr. A60 (2004) 455—464.
[51] J. Kozisek, N.K. Hansen, H. Fuess, Acta Crystallogr. B58 (2002) 463—470.
[52] M. Slouf, A. Holy, V. Petricek, I. Cisarova, Acta Crystallogr. B58 (2002) 519—529.
[53] G.V. Gibbs, Osamu Tamada, M.B. Boisen JR., F.C. Hill, American Minerologist 84 (1999) 435—446.
[54] D. Cremer, E. Kraka, Angew. Chem. 23 (1984) 627—628.
[55] D. Cremer, E. Kraka, Croat. Chem. Acta 57 (1984) 1259.
[56] Enrique Espinosa, Ibon Alkorta, Jose Elguero, Elies Molins, J. Chem. Phys. 117

(2002) 5529–5542.
[57] Alkorta.J. Elguero, C. Foces-Foces, Chem. Commun. (1996) 1633.
[58] I. Rozas, I. Alkorta, J. Elguero, J. Phys. Chem. A102 (1998) 9925.
[59] I. Rozas, I. Alkorta, J. Elguero, J. Phys. Chem. A101 (1997) 9457.
[60] I. Rozas, I. Alkorta, J. Elguero, J. Phys. Chem. A101 (1997) 4236.
[61] A.D. Becke, K.E. Edgecombe, J. Chem. Phys. 92 (1990) 5397–5403.
[62] R. Nesper, Angew. Chem., Int. Ed. Engl. 30 (1991) 789–817.
[63] A. Savin, R. Nesper, S. Wengert, T.F. Fassler, Angew. Chem., Int. Ed. Engl. 36 (1997) 1808–1832.
[64] R.S. Mulliken, J. Chem. Phys. 23 (1955) 1833.
[65] F.L. Hirshfeld, Theor. Chem. Acc. 44 (1977) 129.
[66] T. Lu, F. Chen, J. Theor. Comput. Chem. 11 (2012) 163–183.
[67] Zhang Rui-Zhou, Li Xiao-Hong, Xian-Zhou Zhang, Indian J. Pure Appl. Phys. 49 (2011) 731–739.
[68] C. Lecomte, N.E. Ghermani, V. Pichon-Pesme, M. Souhassou, J. Mol. Struct. 255 (1992) 241–260.
[69] C. Anzline, S. Israel, R. Niranjana Devi, R.A.J.R. Sheeba, P. Richard Rajkumar, Chin. J. Chem. Phys. 30 (2017) 50–62.
[70] M. Arivazhagan, J. Senthil Kumar, Indian J. pure; Appl. phy 50 (2012) 363–373.
[71] V. Petříčěk, M. Dušek, L. Palatinus, JANA, The Crystallographic Computing System, Institute of Physics Academy of sciences of the Czech Republic, Praha, 2006.
[72] M.A. Spackman, J.J. Mckinnon, CrystEngComm 4 (2002) 378.
[73] S.K. Wolff, D.J. Grimwood, J.J. McKinnon, D. Jayatilaka, M.A. Spackman, Crystal Explorer, 2.1, University of western Australia, Perth, 2007.